Master-equation model of a single-quantum-dot microsphere laser

Oliver Benson and Yoshihisa Yamamoto*
ERATO Quantum Fluctuation Project, E. L. Ginzton Laboratory, Stanford University, Stanford, California 94305
(Received 11 December 1998)

We present a theoretical model for the electrically pumped single-quantum-dot microsphere laser. We solve the master equation of the system and analyze the steady state and dynamical properties of the optical field, such as output power, photon number fluctuation, and linewidth, for realistic experimental parameters. The laser threshold power is several orders of magnitude lower than is currently possible with semiconductor microlasers. A semiclassical approximation for the output power and laser linewidth is derived and compared to the exact solution. Electrical pumping together with Coulomb blockade effect allows for the realization of regular pumping in the system. We discuss the possibility for the generation of heralded single photons and of sub-Poissonian laser light. [S1050-2947(99)05506-7]

PACS number(s): 42.55.Sa, 42.55.Px, 42.50.Dv, 78.66.−w

I. INTRODUCTION

Single-atom lasers and single-atom masers have been a subject of intense theoretical and experimental study for several years. They represent the ultimate microscopic limit of lasers and masers in the sense that the active medium consists only of a single atom. Whereas a theoretical treatment of lasers where both the atoms and the light field are quantized usually requires approximations [1], an exact quantum mechanical description is possible in the limit of a single atom. Theoretical models and numerical methods for different configurations were investigated in several papers [2–7].

Experimental realization of these model systems, the single-atom maser [8] and the single-atom laser [9], were used to explore fundamental aspects of light-matter interaction. It was possible to demonstrate the generation of nonclassical states of the electromagnetic field [10] and to study the dynamics of this quantum system in detail [11].

In semiconductor lasers, reducing the volume of the active medium and developing high-Q cavities was motivated by the desire to reduce the laser threshold. An ultimate microscopic limit of semiconductor lasers is a single quantum dot (QD) coupled to a single mode of an optical cavity. An experimental realization of such a single-quantum-dot laser (SQDL) was proposed recently [12]. In contrast to the experimental realizations of the single-atom maser and laser, where dilute atomic beams were utilized, in the SQDL the QD stays in permanent interaction with the laser field. In this sense, it is analagous to the proposed ion-trap laser [13].

Apart from its character as a model cavity-QED system, the SQDL has possible applications as a laser with an ultralow threshold. Low thresholds are of great importance, for example, for applications as low-power optical interconnects in highly integrated structures.

In Sec. II of this paper, we describe our theoretical model for the SQDL. We derive a master equation and show that the model system is equivalent to an incoherently pumped four-level laser. Section III presents the steady state solutions of these equations, and the dependence of the mean photon number, the photon number fluctuations, and the linewidth on the pump rate are discussed for realistic experimental parameters. Due to the short lifetime of the excited QD states, which has to be overcome by strong pumping, self-quenching [3] is a particular problem in the SQDL. We focus on this problem and discuss its effect on the steady state properties. In Sec. IV, we derive a semiclassical approximation for the mean photon number and the linewidth in steady state. Electrical pumping allows for precise control of the pumping process, which is a unique feature of this system. In Sec. V, we show how regular pumping can be implemented in the SQDL. We discuss the possible generation of heralded single photons and of sub-Poissonian laser light.

II. THE MODEL

The system under investigation is a single quantum dot coupled to a single mode of an optical cavity [12]. Figure 1(a) gives a schematic of the experimental setup. The active medium consists of a single self-assembled InAs quantum

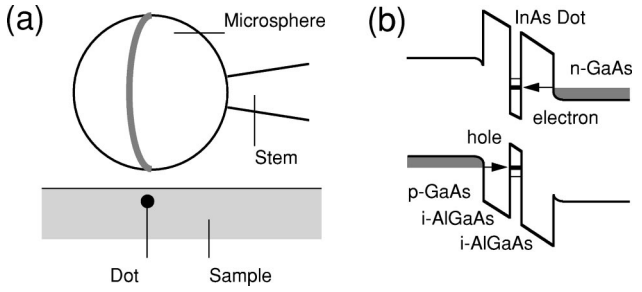

FIG. 1. (a) Schematic of the experimental setup for the single-quantum-dot laser. The active medium consists of a single InAs quantum dot in a GaAs matrix. The optical cavity is a glass microsphere, which is brought close to the sample surface. Light emitted from the dot couples into a whispering gallery mode of the sphere (represented by the equatorial band). (b) Schematic energy-band structure of the double-heterojunction resonant-tunneling structure used for pumping a single quantum dot. Carriers tunnel one at a time from the doped GaAs reservoirs, through the intrinsic AlGaAs barriers, into the isolated InAs QD.

*Also at NTT Basic Research Laboratories, Atsugishi, Kanagawa, Japan.

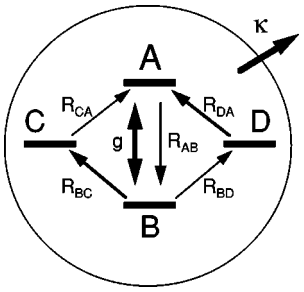

FIG. 2. Schematic level diagram of SQDL laser levels. The four levels are connected via rates R_{BC}, R_{DA}, R_{BD}, and R_{CA} (electron and hole tunneling). Spontaneous emission into nonlasing modes is described by the rate R_{AB}; g is the QD-field coupling constant; and κ is the photon damping rate.

dot in a GaAs matrix. The optical cavity is a glass microsphere, which is brought close to the sample surface. Light emitted from the dot couples into a whispering gallery mode of the sphere.

In our model we assume electrical pumping with unity internal quantum efficiency, ignoring effects such as leakage current. One way to approach this ideal limit is to incorporate the QD into a double-heterojunction resonant-tunneling structure, similar to that used to inject excitons into quantum wells [14]. Figure 1(b) shows a schematic of an appropriate energy-band structure. Carriers can tunnel from the doped GaAs reservoirs, through the intrinsic AlGaAs barriers, into the isolated InAs QD. If an electron (hole) tunnels a second electron (hole) requires a somewhat larger energy to tunnel, due to the Coulomb repulsive energy. The electron (hole) energy level in the QD is effectively shifted by a single electron (hole) tunneling event [thin lines in Fig. 1(b)]. If the shifted energy level lies above the Fermi level of the n (p) side further electron (hole) tunneling is prohibited. This is known as the Coulomb blockade effect. Thus, only a single electron and single hole can tunnel into the electron and hole ground state of the QD. This state, a single hole and a single electron in the QD, is the upper laser state $|A\rangle$. The electron and hole radiatively recombine, leaving the QD in the laser ground state $|B\rangle$, i.e., no hole and no electron in the QD. There are two paths by which to pump the QD to the upper laser state. Either a hole tunnels first, followed by an electron tunneling event, or an electron tunnels first, followed by a hole tunneling event. We denote the intermediate states $|\text{one hole}\rangle|\text{zero electron}\rangle$ and $|\text{zero hole}\rangle|\text{one electron}\rangle$ as states $|D\rangle$ and $|C\rangle$, respectively. Thus, the system can be described as an incoherently pumped four-level laser as depicted in Fig. 2.

The coupling strength of the transition between lasing levels $|A\rangle$ and $|B\rangle$ and the whispering gallery mode of the microsphere (symbolized as a circle in Fig. 2) is determined by the coupling constant g. Incoherent pumping of the upper laser level via intermediate levels $|C\rangle$ and $|D\rangle$ is decribed by rates R_{BC}, R_{CA}, R_{BD}, and R_{DA}. Finally, the rate R_{AB} describes the combined effect of spontaneous emission of photons in modes other than the lasing mode and nonradiative decay, and κ is the damping rate of photons in the laser mode.

The dynamics of the combined QD-field density matrix ρ is governed by the master equation

$$\frac{\partial}{\partial t}\rho=\mathcal{L}\rho=\frac{1}{i\hbar}[H,\rho]+L_{\text{dot}}\,\rho+L_{\text{field}}\,\rho, \tag{1}$$

with the electric dipole, rotating-wave approximation, Jaynes-Cummings Hamiltonian

$$H=-\hbar g(a\sigma^{\dagger}+a^{\dagger}\sigma). \tag{2}$$

Here $\sigma=|B\rangle\langle A|$ and $\sigma^{\dagger}=|A\rangle\langle B|$ are the atomic lowering and raising operators. The cavity mode is assumed to be resonant with the lasing transition, and is described by the boson annihilation and creation operators a and $a^{\dagger}$.

Incoherent pumping and relaxation of the QD levels $|J\rangle$ $(J=A,B,C,D)$ are described by

$$\begin{aligned}L_{\text{dot}}\,\rho=&-\frac{R_{AB}}{2}(|A\rangle\langle A|\rho+\rho|A\rangle\langle A|-2|B\rangle\langle A|\rho|A\rangle\langle B|)\\&-\frac{R_{BC}}{2}(|B\rangle\langle B|\rho+\rho|B\rangle\langle B|-2|C\rangle\langle B|\rho|B\rangle\langle C|)\\&-\frac{R_{CA}}{2}(|C\rangle\langle C|\rho+\rho|C\rangle\langle C|-2|A\rangle\langle C|\rho|C\rangle\langle A|)\\&-\frac{R_{BD}}{2}(|B\rangle\langle B|\rho+\rho|B\rangle\langle B|-2|D\rangle\langle B|\rho|B\rangle\langle D|)\\&-\frac{R_{DA}}{2}(|D\rangle\langle D|\rho+\rho|D\rangle\langle D|-2|A\rangle\langle D|\rho|D\rangle\langle A|),\end{aligned} \tag{3}$$

and the field damping is given by the Liouville operator

$$L_{\text{field}}\,\rho=-\frac{\kappa}{2}(a^{\dagger}a\rho+\rho a^{\dagger}a-2a\rho a^{\dagger}). \tag{4}$$

The equations of motion for the projections of ρ on the QD levels $\rho_{IJ}=\langle I|\rho|J\rangle$ $(I,J=A,B,C,D)$ are easily obtained:

$$\begin{aligned}\frac{\partial}{\partial t}\rho_{AA}&=-ig(\rho_{AB}a^{\dagger}-a\rho_{BA})+(L_{\text{field}}-R_{AB})\rho_{AA}+R_{CA}\rho_{CC}\\&\quad+R_{DA}\rho_{DD},\\\frac{\partial}{\partial t}\rho_{BB}&=-ig(\rho_{BA}a-a^{\dagger}\rho_{AB})+(L_{\text{field}}-R_{BC}-R_{BD})\rho_{BB}\\&\quad+R_{AB}\rho_{AA},\\\frac{\partial}{\partial t}\rho_{AB}&=-ig(\rho_{AA}a-a\rho_{BB})+(L_{\text{field}}-\Gamma)\rho_{AB},\\\frac{\partial}{\partial t}\rho_{BA}&=ig(a^{\dagger}\rho_{AA}-\rho_{BB}a^{\dagger})+(L_{\text{field}}-\Gamma)\rho_{BA},\\\frac{\partial}{\partial t}\rho_{CC}&=(L_{\text{field}}-R_{CA})\rho_{CC}+R_{BC}\rho_{BB},\\\frac{\partial}{\partial t}\rho_{DD}&=(L_{\text{field}}-R_{DA})\rho_{DD}+R_{BD}\rho_{BB},\end{aligned} \tag{5}$$

where $\Gamma = 1/2(R_{AB}+R_{BC}+R_{BD})+\Gamma'$. Γ' describes an additional dephasing rate, which at higher temperatures is mainly due to phonon scattering.

Similarly, the equations of motion for the projections of ρ on the Fock states $\rho_{N,M}=\langle N|\rho|M\rangle$ are

$$\frac{\partial}{\partial t}\rho_{N,M} = -ig(\sqrt{N+1}\sigma^{\dagger}\rho_{N+1,M}+\sqrt{N}\sigma\rho_{N-1,M} - \sqrt{M}\rho_{N,M-1}\sigma^{\dagger}-\sqrt{M+1}\rho_{N,M+1}\sigma) - \frac{\kappa}{2}[(N+M)\rho_{N,M}-2\sqrt{(N+1)(M+1)}\rho_{N+1,M+1}] + L_{\text{dot}}\,\rho_{N,M}\,. \tag{6}$$

These equations could be generalized or modified in order to account for a different or more complicated level structure of the system. Higher excited states of the QD might be involved in a different pumping scheme, and would require additional intermediate states in the pumping system. Coherent optical pumping could also be implemented similar to the case of an optically pumped ion-trap laser [13].

III. STEADY STATE PROPERTIES OF THE SINGLE-QUANTUM-DOT LASER

In this section, we first consider realistic parameters for our calculations, and then discuss the general steady state properties of the SQDL. In our model of the electrically pumped SQDL sketched in Fig. 1, we assume that the resonant-tunneling condition is satisfied simultaneously for electrons and holes. The electron and hole tunneling rates are determined by the design of the double-heterojunction structure, and depend on parameters such as tunnel barrier width and height, doping, and applied bias voltage. Calculations based on the WKB approximation indicate that the ratio of electron tunneling rate (R_{BC} and R_{DA}) and hole tunneling rate (R_{BD} and R_{CA}) is approximately 10 for equal tunnel barrier widths, due to the larger hole effective mass. If the bias voltage is changed, all rates are scanned simultaneously; thus, we assume that the relation $R_{BC}=R_{DA}\approx 10R_{CA}=10R_{BD}$ remains valid. The pump rates R_{BC} range from 500 MHz to over 10 GHz. In the following, we refer to R_{BC} whenever we talk about the pump rate. We would like to point out that the assumption of constant ratios of pump rates is not stringent and that it is straightforward to take into account a more general model, where the pump rates are controlled individually. We will describe such a case in Sec. V. However, the general behavior of the system under consideration is well described by the above assumptions.

Microsphere cavities can be made by melting the tip of an optical fiber with a focused CO_2 laser beam [15]. Q values as high as 3×10^9 have been observed for whispering gallery modes in these spheres. In practice, Q values of 5×10^8 can be readily achieved. This corresponds to a photon damping rate of $\kappa=4$ MHz for 960 nm radiation. Through time resolved photoluminescence experiments [16], the spontaneous decay time R_{AB} in InAs quantum dots was found to be about 650 ps. Finally, in the system considered here, the QD-field coupling constant g can be as large as $g/2\pi=33$ MHz [12].

With these parameters, we use two different methods to solve Eq. (5). The steady state properties are most elegantly derived with the damping basis approach [6]. In this approach, Eq. (5) is expanded in eigenstates of the Liouville operator L_{field}. A recurrence relation can be derived, which is effectively solved by the continued fraction method. A discussion of the damping basis treatment of coupled density-matrix equations can be found in Ref. [4]. Dynamical properties of the SQDL, such as the linewidth and the correlation function, are calculated by numerical integration. We verified our calculations by comparing the steady state results derived by these two independent methods.

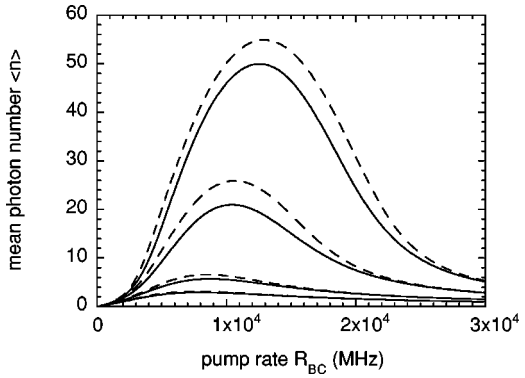

FIG. 3. Dependence of the mean photon number $\langle n\rangle$ in the lasing mode on the pump rate for different photon damping rates κ (from bottom to top $\kappa=6, 5, 4, 3.5$ MHz), coupling strength $g/(2\pi)=31.8$ MHz, and relaxation rate $R_{AB}=1500$ MHz. Dashed curves are semiclassical approximations.

Figure 3 (solid lines) shows the mean photon number in the lasing mode for different photon damping rates κ as the pump rate is changed. The generic behavior for all κ is characterized by an increase in the mean photon number up to a maximum value, followed by a monotonic decrease. This self-quenching [3] was also predicted for incoherently pumped single-atom lasers. It is due to the destruction of the coherence between the lasing levels by the strong incoherent pump. The destruction of coherence can be interpreted in terms of quantum measurement. A continuous measurement is performed, determining wether the QD is in state A or B. The decay rate $\Gamma=1/2\,(R_{AB}+R_{BC}+R_{BD})$ of the coherences ρ_{AB} and ρ_{BA} in Eq. (5) can then be interpreted as the rate of individual measurements.

The threshold of the SQDL can be defined following Björk, Karlsson, and Yamamoto [17]. Laser threshold is reached if the mean number of photons in the lasing mode is one. At this point, stimulated emission overtakes spontaneous emission, and linear amplification is replaced by nonlinear laser oscillation. As can be seen from Fig. 3, threshold can be reached for all values of κ considered.

The Fano factor F,

$$F=\frac{\langle a^{\dagger}aa^{\dagger}a\rangle-\langle a^{\dagger}a\rangle^2}{\langle a^{\dagger}a\rangle}, \tag{7}$$

which measures the relative strength of fluctuations in the photon number, is plotted in Fig. 4 for the same parameters as in Fig. 3. For larger κ, the Fano factor shows a similar behavior as the mean photon number. A maximum of fluctuations coincides with the onset of self-quenching. For

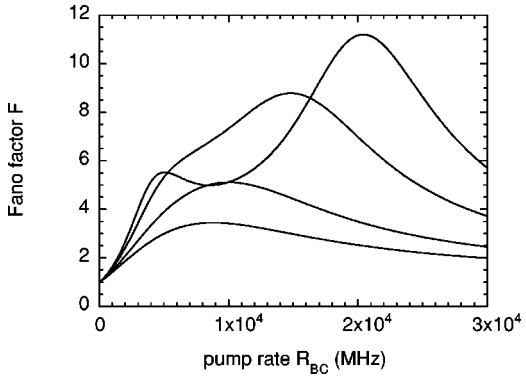

FIG. 4. Dependence of the Fano factor F on the pump rate for different photon damping rates κ (from bottom to top $\kappa = 6, 5, 4, 3.5$ MHz), coupling strength $g/(2\pi) = 31.8$ MHz, and relaxation rate $R_{AB} = 1500$ MHz.

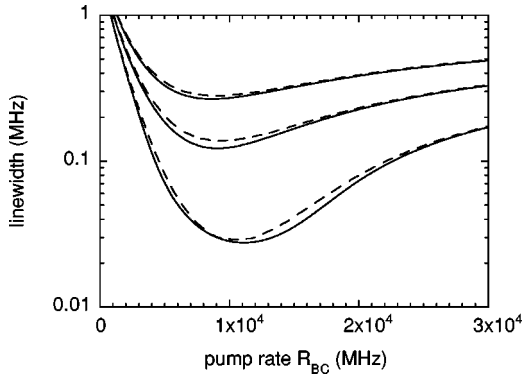

FIG. 5. Calculated linewidth of the SQDL when the pump rate is changed. From bottom to top: $\kappa = 4, 5, 6$ MHz. The other parameters are the same as in Fig. 3. Dashed curves are semiclassical approximations.

smaller κ, the photon number fluctuation curve is characterized by two maximum values close to the laser threshold and to the onset of self-quenching. Decreasing κ results in a wider separation between these two maxima, with a regime of smaller fluctuation in between. The Fano factor outside the cavity F_{out} and inside the cavity F are simply related by $F_{\text{out}} = 1 + 2(F-1)$, if the intensity spectrum is Lorentzian [18]. We verified numerically that this is the case for the parameters used. In contrast to theoretical predictions for single atom lasers, sub-Poisonian statistics (Fano factor below one) are not expected in the SQDL for realistic experimental parameters. This is due to the much smaller ratio of coupling constant g to spontaneous decay rate R_{AB} in the SQDL compared to single-atom lasers.

We calculated the spectrum of the SQDL, which is defined as

$$S(\omega) = \int_0^\infty dt \cos(\omega t) g^{(1)}(t), \tag{8}$$

with the normalized first-order correlation function

$$g^{(1)}(t) = \frac{\langle a^\dagger(t) a \rangle}{\langle a^\dagger a \rangle} = \frac{\text{Tr}\{a^\dagger e^{\mathcal{L}t} a \rho\}}{\text{Tr}\{a^\dagger a \rho\}}. \tag{9}$$

Figure 5 (solid lines) shows the linewidth for the same parameters as in Fig. 3, and for the indicated photon damping rates κ. The linewidth decreases with increasing pump power, marking the transition from amplified spontaneous emission to laser oscillation. For sufficiently high pump rates, self-quenching causes the linewidth to increase until the limit of the empty cavity linewidth is reached.

IV. SEMICLASSICAL APPROXIMATION

In this section, we derive a semiclassical approximation for the mean photon number and the laser linewidth in steady state. This is particularly advantageous for larger photon numbers, where numerical integration becomes too time consuming.

We start with the exact Eq. (5). Due to the short lifetime of the upper laser state in the SQDL, the pump rates have to be large and the photon storage time long in order to achieve threshold. Thus, it is a good approximation to neglect the field damping operator L_{field} in the equation for the polarizations ρ_{AB} and ρ_{BA}. At higher temperatures phonon scattering leads to a large dephasing rate Γ'. Thus, the expectation value $\langle \rho_{AB} \rangle$ can be adiabatically eliminated if the semiclassical factorization of the density matrix is used. This reduces Eq. (5) to an effective two-level system:

$$\begin{aligned}
\dot{\bar{n}} &= \frac{2g^2}{\Gamma}(P_A - P_B)\bar{n} + \frac{2g^2}{\Gamma} P_A - \kappa \bar{n}, \\
\dot{P}_A &= -\frac{2g^2}{\Gamma}(P_A - P_B)\bar{n} - \left(\frac{2g^2}{\Gamma} + R_{AB}\right) P_A + R_{BA} P_B, \\
\dot{P}_B &= -\dot{P}_A,
\end{aligned} \tag{10}$$

where P_A and P_B are the probabilities of finding the QD in state A and B, respectively, $\bar{n}$ is the mean photon number, and $R_{BA} = R_{BC} + R_{BD}$. The effect of the other QD levels involved enters through the normalization condition

$$1 = P_A + P_B + P_C + P_D = P_A + w_B P_B, \tag{11}$$

where we defined the weighting factor w_B, which can be evaluated by inserting the steady state solutions for $P_C = \langle \rho_{CC} \rangle$ and $P_D = \langle \rho_{DD} \rangle$.

The right hand side of Eq. (10) is identical to the rate equations for a semiconductor microlaser derived by Björk and Yamamoto [19] if $(2g^2)/\Gamma(P_A - P_B)$ is replaced by the optical gain in the semiconductor and if the fraction β of spontaneous emission into the lasing mode out of the total spontaneous emission is identified as

$$\beta = \frac{2g^2/\Gamma}{2g^2/\Gamma + R_{AB}}. \tag{12}$$

Here, we are only interested in the steady state properties of the single-quantum-dot laser. In this case it is possible to solve Eq. (5) in steady state, if the semiclassical factorization of the density matrix is used. Thus, for larger photon numbers an approximation for the mean photon number $\bar{n}$ and the populations P_A, P_B, P_C, and P_D can be derived by solving

a quadratic equation. The dashed lines in Fig. 3 correspond to the semiclassical approximation, which reproduces qualitatively the exact calculation. The approximation tends to overestimate the mean photon number by 10–15 % for the values of κ considered.

In Eq. (10), the self-quenching effect enters as a reduction of optical gain when the pump rate is increased. First, if the effective pump rate R_{BA} is small compared to R_{AB}, the optical gain of the laser mode $2g^2/[1/2(R_{AB}+R_{BA})] \approx 2g^2/(1/2R_{AB})$ is nearly a constant. Increasing the pump rate increases the inversion, and thus the mean photon number due to stimulated emission. If the pump rate is further increased, the optical gain will decrease once R_{BA} becomes comparable to R_{AB}. Since the active medium in a SQDL (by definition a single QD) is easily saturated, this decrease in efficiency cannot be overcome by a stronger pumping once a critical pump rate is reached. Beyond this critical rate, which defines the onset of self-quenching, the mean photon number decreases monotonically. It was pointed out in Ref. [3] that this effect is particularly crucial in single-atom lasers because they must be pumped hard to produce a significant amount of light.

We now derive a semiclassical approximation for the SQDL linewidth. Björk and Yamamoto [19] calculate the linewidth $\Delta\nu_{\mathrm{FWHM}}$ of semiconductor microlasers using an equivalent electrical circuit model described in Ref. [20]. Following their approach, and inserting the optical gain of the SQDL, we find

$$\Delta\nu_{\mathrm{FWHM}}=\frac{1}{2\pi}\left(\kappa-\frac{2g^2}{\Gamma}(P_A-P_B)\right), \tag{13}$$

where P_A and P_B are the semiclassical steady state results for the effective two-level system. In Fig. 5, we plot results of the semiclassical approximation as dashed lines. At small pump rates, the linewidth is broadened with respect to the empty cavity linewidth, due to the presence of the absorbing material. In the limit $R_{AB}\gg R_{BA}$, P_A-P_B reduces to $-1/w_B$, as can be derived from Eq. (10), and we find for the linewidth at very small pump rate:

$$\Delta\nu_{\mathrm{FWHM},0}=\frac{1}{2\pi}\left(\kappa+\frac{4g^2}{w_B R_{AB}}\right). \tag{14}$$

Due to the large coupling constant, this broadening is quite significant, even if the absorber is a single QD. At very high pump rate, the QD is completely decoupled from the cavity mode due to self-quenching, and thus the linewidth approaches the empty cavity linewidth $\kappa/2\pi$.

We use the derived approximations for the mean photon number and the linewidth to give a quantitative analysis of the steady state properties of the SQDL for a wider range of photon damping rates κ. Figure 6 shows (a) the normalized output power $P_{\mathrm{out}}/\kappa=\langle n\rangle\hbar\omega$ and (b) the linewidth for $\kappa=4, 3, 2, 1$, and 0.5 MHz, which corresponds to $Q=4.9\times10^8$, 6.5×10^8, 9.8×10^8, 1.9×10^9, and 3.9×10^9, respectively. Above a photon number of unity in the lasing mode, a sharp increase in the photon number and decrease in the linewidth is observed. With increasing Q the onset of self-quenching is shifted to higher pump rates, and there is a larger regime with a linear input/output power characteristic.

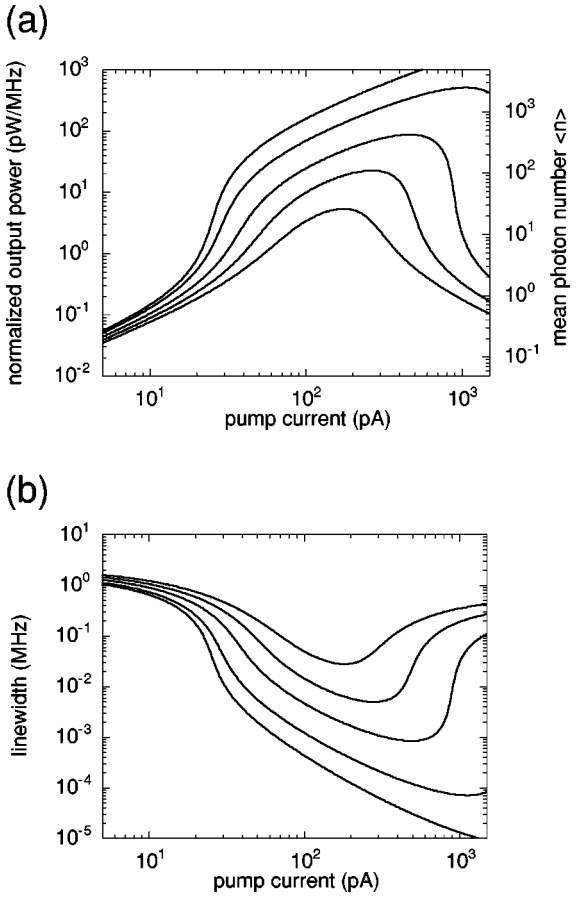

FIG. 6. Semiclassical approximation for (a) the output power and (b) the linewidth for $\kappa=4, 3, 2, 1$, and 0.5 MHz. In (a) the output power is normalized to κ.

The threshold for $\kappa=4$ MHz corresponds to a current of 22.4 pA, more than five orders of magnitude lower than the current record for a microcavity semiconductor laser of 8.7 μA [21]. The maximum output power of 16.5 pW in this case can be increased to several nW by increasing the Q of the optical cavity.

V. REGULAR PUMPING

In the electrically pumped SQDL, the Coulomb blockade effect together with resonant tunneling can be utilized to control electron and hole tunneling individually. Figure 7(a) shows the schematic energy-band structure when the resonant-tunneling condition is satisfied for electrons and holes at different bias voltages V. Due to the Coulomb blockade effect, one and only one electron tunnels at $V=V_e$, and one and only one hole tunnels at $V=V_h$. In this case, the level scheme of the SQDL can be reduced to the three-level scheme shown in Fig. 7(b). Starting with the SQDL ground state $|B\rangle$ (no hole and no electron in the QD), the bias voltage is set to the electron resonant-tunneling condition, and an electron can tunnel (intermediate state $|C\rangle$). Then, the voltage is switched to satisfy the hole resonant-tunneling condition, and a hole can tunnel (upper SQDL state $|A\rangle$), followed by the emission of a single photon. By modulating the applied bias voltage between V_e and V_h, a single electron and a single hole can be injected per modulation period T, as

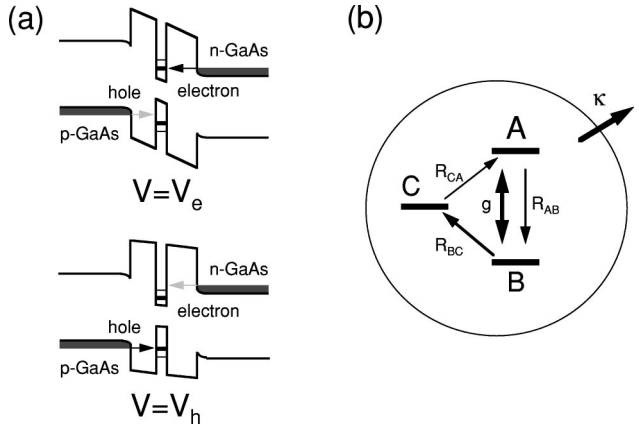

FIG. 7. (a) Schematic energy-band structure of the double-heterojunction resonant-tunneling structure when the resonant-tunneling condition is satisfied for electrons and holes at different bias voltages $V=V_e$ and $V=V_h$. (b) Schematic level diagram of the SQDL laser in this situation. Periodic switching between $V=V_e$ and $V=V_h$ results in a periodic switching between the situations $R_{BC}=0$, $R_{CA}\neq 0$ and $R_{CA}=0$, $R_{BC}\neq 0$.

long as the electron and hole tunneling rates are large compared to the modulation frequency $f=1/T$. Thus, regular pumping is realized. Another regular pumping scheme utilizing surface acoustic waves was proposed recently [22]. There are two operation regimes, depending on whether the modulation frequency is smaller or larger than the photon damping rate of the optical cavity.

In the first case, the photon damping rate is larger than the modulation frequency. The mean photon number in the cavity is much smaller than one, and the laser is far below threshold. If, in this case, the spontaneous emission rate is large compared to the modulation frequency, a single photon is emitted within each cycle. Thus, a stream of single photons with well regulated time intervals can be generated. Experimental evidence for such a single photon turnstile device [23] was given recently [24]. The device used in this experiment consists of an intrinsic quantum well as an active medium in the middle of a mesoscopic p-n junction. The experiment was performed at 50 mK, where the Coulomb repulsive energy between electrons or holes dominates over thermal fluctuations. Turnstile operation in a SQDL setup, where a single QD is coupled to a high-Q optical cavity, is superior for two reasons. First, the Coulomb repulsive energy between electrons or holes is larger in a single QD because of its small size. Coulomb blockade and turnstile operation is thus possible at higher temperatures. Second, the spatial emission pattern and the spontaneous emission rate are modified due to the presence of the optical cavity, which allows for a better output coupling of the emitted light and a higher modulation frequency.

In the second regime, the photon damping rate is smaller than the modulation frequency. Photons can be stored in the optical cavity, and lasing is possible. In order to demonstrate the transition from phase-incoherent, heralded single-photon emisson to phase-coherent laser light, we calculated the intensity autocorrelation function $g^{(2)}$,

$$g^{(2)}=\langle a^{\dagger}a^{\dagger}(t)a(t)a\rangle=\mathrm{Tr}\{a^{\dagger}ae^{\mathcal{L}t}a\rho a^{\dagger}\}, \qquad (15)$$

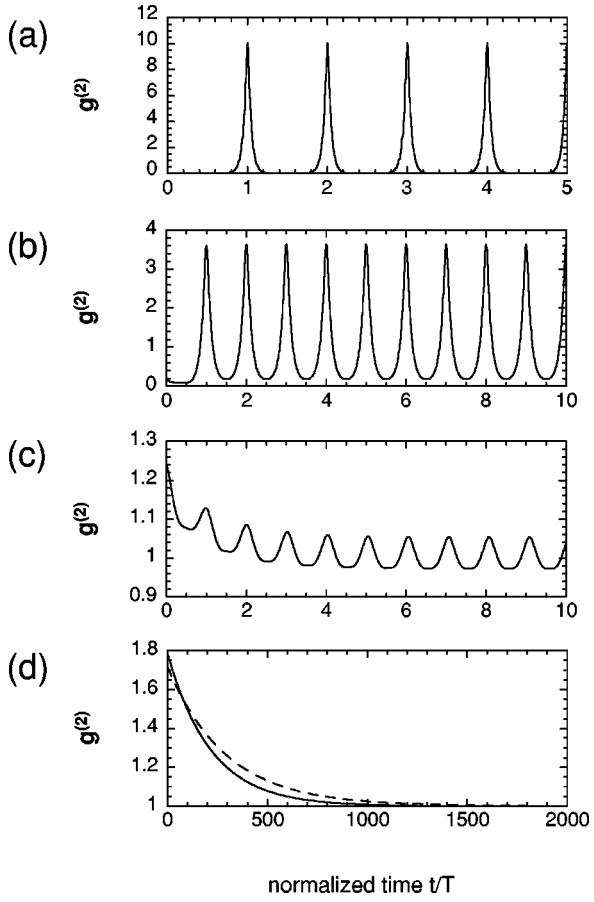

FIG. 8. Second-order correlation function $g^{(2)}$ for different modulation frequencies f. (a) $\beta f=0.016\kappa$, (b) $\beta f=0.05\kappa$, (c) $\beta f=0.16\kappa$, (d) $\beta f=1.6\kappa$. For all curves $\kappa=5$ MHz, $\beta=0.016$, $g/(2\pi)=31.8$ MHz, $R_{BC}=10^4$ MHz, and $R_{AB}=1500$ MHz. The time is normalized to $T=1/f$.

and the linewidth of the emitted light via numerical integration.

Figure 8 shows the calculated $g^{(2)}$ for four different driving frequencies f. All curves are normalized by the mean photon number averaged over many periods T. The emission rate of photons into the laser mode is βf if the rates R_{BC} and R_{CA} are larger than the driving frequency f. In the upper curve, Fig. 8(a), βf is much smaller than the photon damping time $1/\kappa$. The photons in the laser mode are antibunched; i.e., the probability to find a second photon succeeding a given photon is zero within a time interval T. Furthermore, photon emission events occur at regular time intervals T. In this low-frequency limit, the SQDL runs in a turnstile mode. The fluorescence light is a stream of single photons with well regulated time intervals.

When f is increased [Fig. 8(b)–8(d)], the mean number of photons in the laser mode starts to increase once βf becomes comparable to or larger than $1/\kappa$. The regulated photon stream evolves into phase-coherent SQDL light. The $g^{(2)}$ function finally approaches the steady state value calculated for a continuously pumped three-level laser (with one-half of the pump rate) which is plotted as a dashed line in Fig. 8(d). The dependence of the linewidth on the driving frequency f is shown in Fig. 9. The transition from phase-incoherent single-photon emisson to phase-coherent laser light is ob-

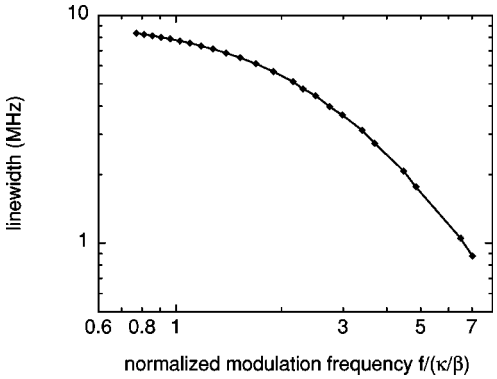

FIG. 9. Dependence of the linewidth on the driving frequency *f*. *f* is normalized to κ/β.

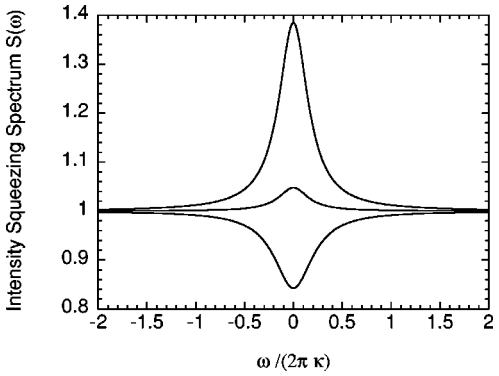

FIG. 10. Intensity squeezing spectrum outside the cavity for (from top to bottom) $\eta=0.86$, 0.87, and 0.89, which correspond to $g/(2\pi)=47.7$, 50.9, and 55.7 MHz, respectively. The photon damping rate κ is 4 MHz, the decay in nonlasing modes $R_{AB}=1500$ MHz, and $R_{BC}=R_{CA}=10^4$ MHz. The frequency $\omega/(2\pi)$ is normalized to κ.

served as a linewidth narrowing. In the low-frequency limit the linewidth is determind by the linewidth of the cavity containing an absorbing material. With increasing frequency the linewidth decreases and approaches the steady state linewidth of a continuously pumped three-level laser.

In the calculation shown in Fig. 8(d), the electron and hole tunneling rates are large compared to the modulation frequency $f=1/T$. As mentioned above, this is the regime of a regularly pumped laser, and the pump noise introduced is very small. The situation is similar to a semiconductor in constant current operation [25], where the minority carrier number is modulated freely by spontaneous emission, stimulated emission, and absorption processes. However, for the parameters used in the calculation shown in Fig. 8(d), the fraction η of emission (spontaneous and stimulated) into the lasing mode out of the total spontaneous emission is much smaller than one ($\eta=0.024$). Thus, the noise introduced by spontaneous emission into nonlasing modes is large. This noise can be suppressed by increasing the photon number, and thus stimulated emission, or by decreasing the spontaneous emission in other modes due to the geometry of cavity. In order to demonstrate that sub-Poissonian light generation is possible in the SQDL, we calculated the intensity squeezing spectrum outside the cavity [26]

$$S(\omega)=1+4\kappa\left\{\mathrm{Re}\left[\int_0^\infty dt\,\exp(i\omega t)(g^{(2)}-\langle n\rangle)/\langle n\rangle\right]\right\} \tag{16}$$

for different values of η. The results are shown in Fig. 10. If η is small, super-Poissonian light $[S(\omega)>1]$ is produced. This is also the case for the parameters used for the calculaton in Fig. 8(d). With increasing η, a transition from super-Poissonian to sub-Poissonian $[S(\omega)<1]$ light is observed. In practice, η can be inreased by increasing the Q value of the optical cavity and by increasing the coupling strength g between QD and the lasing mode [12].

VI. CONCLUSION

We gave a theoretical model for the electrically pumped single-quantum-dot laser. The model is equivalent to an incoherently pumped four-level laser. Laser oscillation can be obtained in this system for realistic experimental parameters. As mentioned, it is straightforward to account for a different or more complicated level structure in this system. This would be the case for the implementation of optical pumping, which might be easier to achieve in a first experiment. However, electrical pumping allows for precise control of the pumping process via the Coulomb blockade effect. This unique feature of the SQDL laser is very attractive for possible applications, and allows for interesting experiments to study a regularly pumped cavity-QED system.

ACKNOWLEDGMENTS

We would like to thank Matthew Pelton for valuable discussions. O.B. acknowledges financial support from the Alexander von Humboldt Foundation.

[1] H. Haken *Laser Theory* (Springer-Verlag, Berlin, 1984).
[2] G.S. Agarwal and S.D. Gupta, Phys. Rev. A **42**, 1737 (1990).
[3] Yi. Mu. and C.M. Savage, Phys. Rev. A **46**, 5944 (1992).
[4] C. Ginzel, H.-J. Briegel, U. Martini, B.-G. Englert, and A. Schenzle, Phys. Rev. A **48**, 732 (1993).
[5] T. Pellizzari and H. Ritsch, J. Mod. Opt. **41**, 609 (1994); P. Horak, K.M. Gheri, and H. Ritsch, Phys. Rev. A **51**, 3257 (1995).
[6] H.J. Briegel and B.-G. Englert, Phys. Rev. A **47**, 3311 (1993).
[7] H.-J. Briegel, G.M. Meyer, and B.-G. Englert, Europhys. Lett. **33**, 515 (1996).
[8] D. Meschede, H. Walther, and G. Müller, Phys. Rev. Lett. **54**, 551 (1985).
[9] K. An, J.J. Childs, R.R. Dasari, and M.S. Feld, Phys. Rev. Lett. **73**, 3375 (1994).
[10] G. Rempe, F. Schmidt-Kaler, and H. Walther, Phys. Rev. Lett. **64**, 2783 (1990).
[11] O. Benson, G. Raithel, and H. Walther, Phys. Rev. Lett. **72**, 3506 (1994).

[12] M. Pelton and Y. Yamamoto, Phys. Rev. A **59**, 2418 (1999).
[13] G.M. Meyer, H.-J. Briegel, and H. Walther, Europhys. Lett. **37**, 317 (1997).
[14] H. Cao, G. Klimovitch, G. Björk, and Y. Yamamoto, Phys. Rev. Lett. **75**, 1146 (1995).
[15] L. Collot, V. Lefevre-Seguin, M. Brune, J.M. Raimond, and S. Haroche, Europhys. Lett. **23**, 327 (1993).
[16] G. Solomon, M. Pelton, and Y. Yamamoto (unpublished).
[17] G. Björk, A. Karlsson, and Y. Yamamoto, Phys. Rev. A **50**, 1675 (1994).
[18] H. Ritsch, P. Zoller, C.W. Gardiner, and D.F. Walls, Phys. Rev. A **44**, 3361 (1991).
[19] G. Björk and Y. Yamamoto, IEEE J. Quantum Electron. **72**, 2386 (1991).
[20] A. Yariv, *Quantum Electronics* (Wiley, New York, 1989).
[21] G.M. Yang, M.H. MacDougal, and P.D. Dapkus, Electron. Lett. **31**, 886 (1995).
[22] C. Wiele, F. Haake, C. Rocke, and A. Wixforth, Phys. Rev. A **58**, R2680 (1998).
[23] A. Imamoğlu and Y. Yamamoto, Phys. Rev. Lett. **72**, 210 (1994).
[24] J. Kim, O. Benson, H. Kan, and Y. Yamamoto, Nature (London) **397**, 500 (1999).
[25] W. Richardson and Y. Yamamoto, Phys. Rev. A **44**, 7702 (1991).
[26] D. F. Walls and G. J. Milburn, *Quantum Optics* (Springer-Verlag, Berlin, 1994).